

Snow Avalanche Frequency Estimation (SAFE): 32 years of monitoring remote avalanche depositional zones in high mountains of Afghanistan

Arnaud Caiserman^{1*}, Roy C. Sidle¹, Deo Raj Gurung²

¹ Mountain Societies Research Institute – University of Central Asia, Khorog, 736000, Tajikistan

A. Caiserman ORCID: <https://orcid.org/0000-0003-4580-6633> ; corresponding author: arnaud.caiserman@ucentralasia.org

Roy C. Sidle ORCID: <https://orcid.org/0000-0002-5004-4154>

² Aga Khan Agency of Habitat, Dushanbe, 734013, Tajikistan

Correspondence to: Arnaud Caiserman (arnaud.caiserman@ucentralasia.org)

Abstract. Snow avalanches are the predominant hazards in winter in high elevation mountains. They cause damage to both humans and assets but cannot be accurately predicted. Here we show how remote sensing can accurately inventory large avalanches **depositional** zones every year in a large basin using a 32-y snow index derived from Landsat satellite archives. This Snow Avalanche Frequency Estimation (SAFE) built in an open-access Google Engine script maps snow hazard frequency and targets vulnerable areas in remote regions of Afghanistan, one of the most data-limited areas worldwide. SAFE correctly detected of the actual **depositional zones** of avalanches identified on Google Earth and in the field (Probability of Detection 0.77 and Positive Predictive Value 0.96). A total of 810,000 large **depositional zones** of avalanches occurred since 1990 within an area of 28,500 km² with a mean frequency of 0.88 avalanches^{km²y⁻¹}, damaging villages and blocking roads and streams. Snow avalanche frequency did not significantly change with time, but a northeast shift of these hazards was evident. SAFE is the first robust model that can be used worldwide and is especially capable of filling data voids on snow avalanche impacts in inaccessible regions.

1. Introduction

Snow avalanches are among the fastest, up to 61 m s⁻¹, and therefore most dangerous natural hazards in mountain areas (Louge et al., 2012). Casualties associated with avalanches are numerous; in 2021 alone, 37 fatalities occurred in the US (Colorado Avalanche Information Center, 2021) and 127 in Europe (European Avalanches Warning Services, 2021), but avalanche monitoring is not consistent across the globe. Most remote mountain regions and communities are not systematically monitored for avalanche occurrence. Avalanche surveys amongst remote villages are sparse because regions are uninhabited; however, avalanches can block connecting roads every year since avalanche volumes range from hundreds to several tens of thousand cubic meters (Gubler, 1987). Where weather stations exist, avalanches can be predicted based on snow depth and other weather parameters (Greene et al., 2016). However, the global weather monitoring of mountainous areas is scattered and very sparse in developing nations.

33 To support these science and government priorities in remote mountain regions, it is necessary to introduce a user-
34 friendly, open-access method that maps snow avalanches on an annual basis across wide areas where internet
35 connection and monitoring systems are not always available. As an example, half of the land surface of
36 Afghanistan is above 2000 m a.s.l. and 80% is mountainous (Asad Sarwar, 2002). Among Central Asian nations,
37 Afghanistan's population is most at risk of avalanche hazards; 22,477 inhabitants at risk compared to 5183 in
38 Tajikistan (Chabot and Kaba, 2016). Particularly, northeast Afghanistan (Badakhshan) is one of the most
39 vulnerable regions, especially from December through March (Mohanty et al., 2019). Several international
40 initiatives have been implemented in Afghanistan to forecast avalanches or assess their risks on local communities.
41 According to USAID, 30,600 buildings are at risk of avalanches in Badakhshan based on daily snow depth
42 measurements (USAID, 2021). The Aga Khan Agency for Habitat (AKAH) collects snow depth data and uses
43 models such as Alpine3D and SNOWPACK to forecast avalanche prone regions in Tajikistan, Afghanistan, and
44 Pakistan (Bair et al., 2020). Other products have been developed, such as avalanche susceptibility and exposure
45 maps (Kravtsova, 1990; Soteres et al., 2020; World Bank, 2017). Another approach is to combine topographic
46 maps and snow data via the RAMMS:AVA models (GFDRR, 2018), but these are not open access. Finally, it is
47 possible to count the number of avalanches in each district as done by the United Nations in their map *Districts*
48 *Affected by Avalanches* (OCHA-United Nations, 2012), but this is time consuming and may miss some events
49 across large areas.

50
51 Detecting the avalanches is a challenge and requires temporal as well as spatial data, especially for large areas.
52 Remote sensing technology, both air and spaceborne, can cover large areas at different times of the year. Indeed,
53 the frequent collection of satellite images over the same area enables the detection of changes in snow cover as
54 well as other hazards, such as floods and landslides. Until recently, the use of remote sensing in avalanche detection
55 was sparse due to low resolution, and the automation of such processes was even more difficult because of the
56 lack of relevant algorithms that can compute big data (Eckerstorfer et al., 2016). Other remote sensing approaches
57 for avalanche detection have used radar, Lidar, and optical data. Radar satellites, such as Sentinel-1A and B, are
58 now commonly used for detecting mass movements by assessing backscatter signal changes between two time
59 periods (before and after movement) by a co-registration of the two images. Backscatter values provide
60 information on terrain roughness and any change indicates that a mass movement or a significant erosion event
61 occurred in a given area. **Vickers et al. (2016) conducted one of the first studies utilizing Sentinel-1 products to
62 detect avalanches debris by developing an unsupervised classification.** This technology seems very promising for
63 avalanche detection (Eckerstorfer et al., 2017; Malnes et al., 2015; Martinez-Vazquez and Fortuny-Guasch, 2008;
64 Schaffhauser et al., 2008; Tompkin and Leinss, 2021; Yang et al., 2020). **Using TerraSAR-X and Sentinel-1
65 products, Leinss et al. (2020) mapped avalanches, demonstrating the potential of radar products in snow hazard**

66 detection. However, the acquisition of frequent radar images is too recent to use this technique to detect historical
67 avalanches. In addition to optical, radar or Lidar data, other studies used Digital Elevation Models (DEMs) and
68 topographic parameters to determine the influence of terrain on avalanches in Switzerland (Maggioni and Gruber,
69 2009). Other studies incorporated other parameters such as morphology and vegetation to define potential
70 avalanche zones and ran the Avalanche Flow and Run-out Algorithm to automatically detect potentially affected
71 regions by avalanches (Barbolini et al., 2011). Moreover, the combination of snow measurements (depth) and high
72 resolution DEMs have proved useful in snow hazard detection (Bühler et al., 2018a, 2022). Lidar is being used in
73 the same regard with a higher level of precision. Lidar sensors measure snow depth before and after events at
74 submeter resolutions (Prokop, 2008; Deems et al., 2013; Prokop et al., 2013; Hammond et al., 2018). However,
75 this technology remains very expensive, and the spatial coverage is limited. Therefore, Lidar data are not suitable
76 for avalanche detection at the basin scale. In addition to optical, radar or Lidar data, other studies used Digital
77 Elevation Models and topographic parameters to determine the terrain influence on avalanches in Switzerland
78 (Maggioni and Gruber, 2009). Some other studies added other parameters such as morphology and vegetation to
79 define potential avalanche zones and ran Avalanche Flow and Run-out Algorithm to automatically detect regions
80 that are potentially affected by avalanches (Barbolini et al., 2011). Moreover, the combination of snow
81 measurements (depth) and high resolution DEMs was shown to be efficient for snow hazard detection (Bühler et
82 al., 2018a).

83

84 Optical data are the most available data in terms of spatial and temporal resolution as well as historical archives.
85 Thus, we used optical data to detect avalanches on a long-term basis. Landsat-5, 7 and 8 products were used as
86 their resolution (30 m, 900 m²) is sufficient to detect small avalanches (Eckerstorfer et al., 2016). Most of these
87 data are available at a global scale. Optical sensors can detect areas covered or not covered by snow and this
88 approach has been used in multiple studies during the past decade. Manual approaches or indices have been used
89 in such studies. For example, Landsat-8 Panchromatic images (15 m) in combination with radar images were used
90 to detect avalanches in Norway (Eckerstorfer et al., 2014). Such combinations were also recently used in west
91 Greenland to map a large number of avalanches after an unprecedented snow event (Abermann et al., 2019). To
92 our knowledge, only one recent study automated the detection of avalanches using remote sensing products and
93 an open-access scripting approach (Smith et al., 2020). This study downloaded avalanches annually for a given
94 region of interest using available Landsat-8 images and computed NDSI for each image. NDSI differentiated so-
95 called 'supraglacial debris' from snow cover, for the date of interest. However, this approach only covers high
96 elevation areas while our study aims to detect avalanches proximate to local communities at lower elevations
97 (typically valleys). Manual and visual approaches, despite the time consuming process, can also be applied to
98 detect avalanches using high resolution images (e.g., SPOT-6), mid-resolution (e.g., Sentinel-2A and B images),

99 or even Google Earth images (Singh et al., 2020; Yariyan et al., 2020; Hafner et al., 2021). **Across a wide area**
100 **(12,500 km²) individual snow avalanches were manually digitized using high resolution SPOT-6 images** (Bühler
101 et al., 2019a). Terrain parameters like slope gradient and curvature have also been added to the avalanche detection
102 process using DEMs (Soteres et al., 2020) combined with Landsat-8 images (Bühler et al., 2018b; Singh et al.,
103 2019). Integrated criteria are therefore recommended to detect avalanches. To our knowledge, no long-term
104 avalanche mapping studies using remote sensing have been conducted in the world, especially not in Afghanistan.
105

106 The general objective of this study is to map annual **depositional** zones of avalanche occurrence over the past 32
107 years using Landsat image archives in Badakhshan region, Afghanistan. Such long-term monitoring is the first
108 attempt globally and enables us to map the frequency of **depositional** zones of avalanches that impact valley
109 communities. Thus, we used optical data to detect **depositional** zones on a long-term basis and built an open-access
110 script in Google Engine interface: *Snow Avalanche Frequency Estimation (SAFE)*. Landsat-5, 7 and 8 products
111 were used as their resolution (30 m, i.e., minimum detectible size of 900 m²) is sufficient to detect larger avalanches
112 (Abermann et al., 2019; Eckerstorfer et al., 2014, 2016; Hafner et al., 2021; Singh et al., 2019, 2020; Smith et al.,
113 2020; Yariyan et al., 2020). Our objective is to automatically map annual **depositional** zones of avalanche
114 occurrence over the past 32 years using Landsat-5, 7 and 8 image archives in the Amu Panj basin of Afghanistan.
115 **SAFE is applicable in all high mountains worldwide, such as the Tien Shen, Himalaya, Hindu Kush, Karakoram**
116 **or Andes, but not restricted to these, where snow avalanche deposits can be detected prior to melting every year**
117 **across a multi-annual spectrum using satellite images.** These outputs are of keen interest to decision makers who
118 can use this automated process to map avalanche hazard in the future. The most vulnerable areas, villages and
119 roads, were mapped to improve future planning. In addition, this research enables the monitoring of **depositional**
120 zones of avalanche evolution over the past 32 years. Such analyses should strengthen local community resilience
121 to snow avalanches.
122

123 **2. Materials and methods**

124 *2.1 Study area*

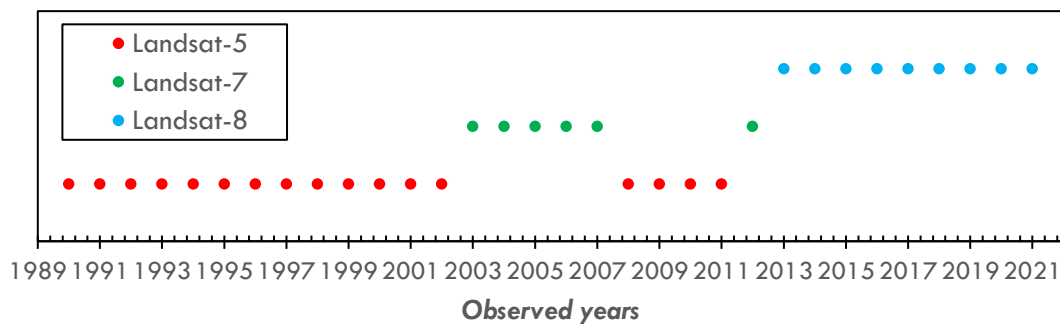
125 The study covers the most mountainous region of Afghanistan – Badakhshan in the Amu Panj basin located in the
126 northeast portion of the country. Average elevation is 2761 m and mean slope gradient is 21%. This region spans
127 from Bamyan Province to the Hindu Kush range, up through the Wakhan corridor in the far east of Afghanistan.
128 The summit is Nowshak Peak at an elevation of 7492 m a.s.l. The western part of Amu Panj basin is rather flat
129 and not prone to avalanches. Annual precipitation is about 600 mm occurring mostly as snow between February
130 and May (Zhang et al., 2015). This terrain and precipitation characteristics lend Badakhshan very prone to
131 avalanches. The basin is large (28,580 km²), justifying automated avalanche detection to cover this area in a

132 reasonable amount of time using Google Engine. Despite the remoteness of this region, Badakhshan has a
133 population of 950,953 inhabitants (Islamic Republic of Afghanistan Governmental Website, 2021) distributed in
134 4154 villages, mainly in valleys. However, 35% of the villages in Badakhshan are located at elevations above 2000
135 m, increasing the vulnerability of these communities to avalanches.

136

137 2.2 Landsat archives for snowpack analysis

138 This analysis requires the integration of numerous data into a Google Engine Java script. Firstly, a mosaic of
139 different Landsat images is created every year in the Amu Panj basin. Depending on the year of interest, Landsat-
140 5 (https://developers.google.com/earth-engine/datasets/catalog/LANDSAT_LT05_C02_T1_L2), Landsat-7
141 (https://developers.google.com/earth-engine/datasets/catalog/LANDSAT_LE07_C02_T1_L2) or Landsat-8
142 (https://developers.google.com/earth-engine/datasets/catalog/LANDSAT_LC08_C02_T1_L28) images were
143 downloaded. Within a given year the same satellite images were used. Before 1990, coverage by Landsat-5 was
144 insufficient in this region of Afghanistan. Landsat images were directly downloaded from Google Engine Archives
145 under their *ImageCollection*. Depending on the availability of images and the year of interest, one satellite or
146 another was used (Figure 1).



147

148 **Figure 1. Landsat archives used for depositional zones of avalanches detection since 1990.**

149

150 2.3 Shuttle Radar Topography Mission-30 for terrain selection

151 Detecting **avalanche deposits** requires terrain parameters defined by using the Shuttle Radar Topography Mission-
152 30 (<https://dwtkns.com/srtm30m/>) This Digital Elevation Model was collected in 2000 and is globally available on
153 the United States Geological Survey data portal at a spatial resolution of 30 m. SRTM-30 is used in this study to
154 delineate the regions of interest by deriving stream channels from the DEM.

155

156

157

158 *2.4 Terra MODIS MOD10A2.006 for snow line analysis*

159 The ROI (regions of interest) are delineated using Terra MODIS MOD10A2.006
160 (<https://nsidc.org/data/MOD10A2/versions/6>). This product of MODIS shows the snow cover (baseline: 8 days)
161 and is also globally available at a resolution of 500 m. MOD10A2.006 snow cover data are available since 2000.
162 MODIS is used to extract the seasonal snow line elevations (average) during the past 20 years in the Amu Panj
163 basin.

164

165 *2.4 Terra MODIS MOD11C3.006 for land surface temperature analysis*

166 The evolution of land surface temperature was completed using MOD11C3.006 monthly products, 0.05 degrees
167 (<https://lpdaac.usgs.gov/products/mod11c3v006/>). Temperature trends were analysed from 2000 through 2021
168 (significance > 0.05 p-value) and the slopes were extracted and plotted on monthly maps.

169

170 *2.6 Concept of the SAFE algorithm*

171 As the aim of this study is to detect and map the annual occurrence of **depositional** zones during the past 32 years
172 within the study area, the monitoring approach must be reasonable and transferable from year to year. Based on
173 frequent field observations and literature (Eckerstorfer et al., 2016), the authors noticed that **depositional** zones
174 can be detected using the contrast between snow cover and bare cover, but the timing is perhaps the most important
175 consideration. Indeed, the script is based on the assumption that snow packages exist in lowlands, especially along
176 rivers and streams, as late as May through mid-July. At this time of the year, the terrestrial snow cover has largely
177 melted and only snow packages triggered by avalanches remain. The location of those snow packages is also very
178 critical (i.e., along riverbanks). These zones are indeed detectable by delineating the **depositional zones of the**
179 **avalanches** (not their release or transition zones); in most cases these were located on river or stream banks as
180 observed in the field because the hillslopes always route snow avalanches in this direction. We cannot differentiate
181 between dry, wet, or powder snow because the process detects the remaining snow packages as avalanches in the
182 late season (spring and summer), not in winter, nor can we delineate multiple **deposits** within the same depositional
183 feature, only the combined **deposit zones**. In winter, we were not able to differentiate contrasts between snow cover
184 and avalanches, thus our focus is on the late season.

185

186 *2.7 Google Engine interface and code availability*

187 The concept of detecting the ‘remaining snow avalanches deposits in the late season’ was written in Java Script
188 using the *Google Engine* platform. The script SAFE is available at
189 <https://code.earthengine.google.com/2a3bc50702a76d6989119a4a6c07af80>. We selected *Google Engine* for its
190 relative simplicity of use and open access code, which is available to all stakeholders involved in hazard and

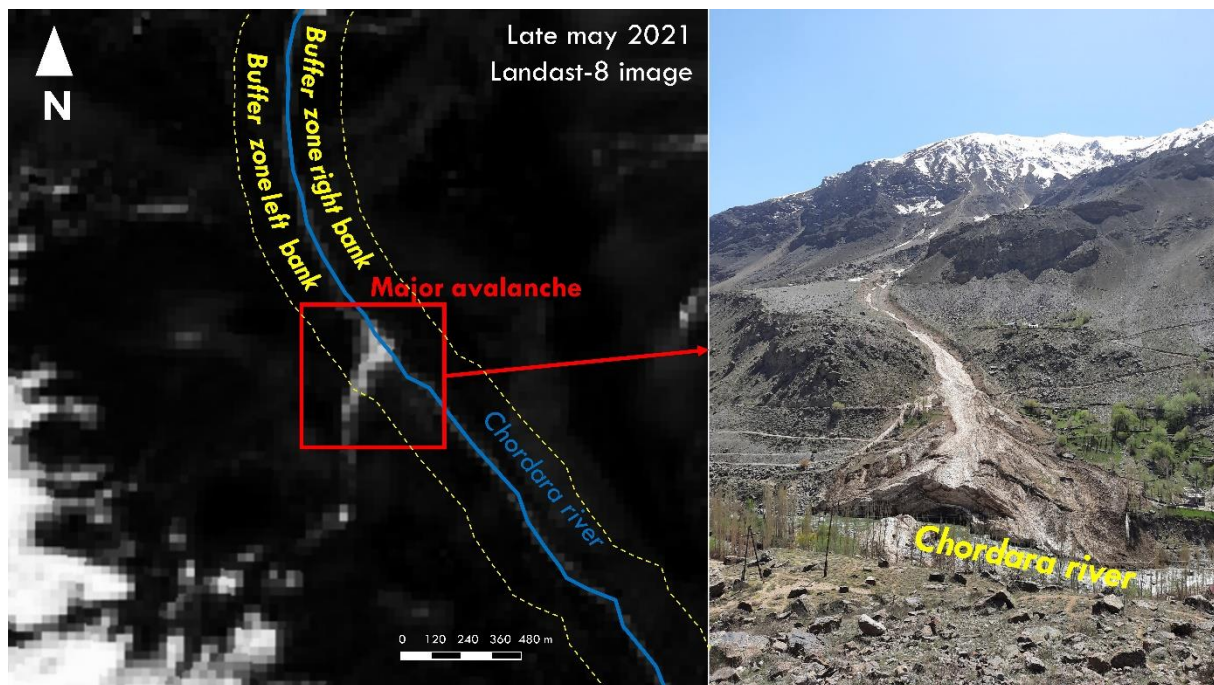
191 vulnerability assessments. Additionally, internet connections in remote areas, such as within the Amu Panj basin,
192 are limited and powerful computers required to run scripts and process big data are sparse. Our script can be run
193 by anyone in a reasonable amount of time, even with a low internet capacity. As an example, yearly **depositional**
194 **zones of avalanches** in our study area were downloaded and mapped from Badakhshan (SAFE was processed from
195 Khorog, University of Central Asia campus, in Tajikistan) in 11.3 h (about 20 min per year of record) with an
196 average connection of 2.2 Gb/s.

197

198 2.8 Region of interest

199 The first step of SAFE is to define a region of interest as a mask to clip the Landsat images using SRTM-30 and
200 MOD10A2.006. Avalanche deposits that terminated on riverbanks, rivers, and streams are derived from SRTM-
201 30 DEMs using *ArcHydroTool* in *ArcGIS Pro Software*. Buffers of 200 m on both sides of rivers and streams are
202 defined to: (1) catch the depositional zone of avalanches that terminate in rivers and (2) increase the probability of
203 excluding the snow coverage in higher elevations that may remain throughout the summer. As an illustration, a
204 major avalanche occurred in the border zone of Afghanistan and Tajikistan in winter 2021. The remaining
205 depositional zone was still distinct in late May and June of that year on the bank of Chordara River (Figure 2).

206



207

208 **Figure 2. An illustration of avalanche **depositional zone** detection using late snow season Landsat-8 image**

209

near Khorog in May 2021 (Badakhshan in Tajikistan)

210 *2.9 Date range of interest*

211 A 200 m riparian buffer was used as a mask to clip the Landsat images. Because our area of coverage encompasses
212 very different elevations, the date of snow melt is not uniform throughout the basin. Therefore, distinguishing
213 between the depositional zone and bare land requires different times depending on elevation. To accomplish this,
214 we calculated the average elevation of the snowline for the last 20 years using MODIS products. To distinguish
215 the different melt timing between highlands from lower areas, we selected the summer snowline (June-July-
216 August; JJA). The average elevation of the JJA snowline was 4420 m during the past 20 years. Two masks were
217 therefore produced: one with a river buffer in lowlands and another for highlands. Those masks are only relevant
218 if the user carefully selects the date of interest. For lowlands (below 4420 m), our time window was 15 May to 15
219 June, indicating that the script downloads and compiles all available Landsat images acquired in this range and
220 detects the **deposit zones** efficiently because during that period the terrestrial snow cover has already melted and
221 the deposits are easily recognised. For higher elevations (above 4420 m), snow cover melted later; dates to
222 accurately distinguish the remaining snow packages ranged from 15 June to 15 July. After many tests, it was
223 confirmed that these date ranges reproduced the desired snow conditions during the entire 32-y period. In the
224 script, users can modify these dates (lines 24 and 112) to conform to local conditions.

225

226 *2.10 Snow index reclassification*

227 After the construction of the mask, SAFE proceeds as outlined in Figure 3. NDSI is selected to detect snow of
228 **deposit zones** in the script for its transferability from one Landsat generation to another. NDSI computes a ratio
229 between VIS and SWIR bands of Landsat satellites with negative NDSI representing non-snow cover and positive
230 values indicating snow coverage (Equation 1). Three cover types were distinguished to detect **depositional zones**
231 **of avalanches** at the correct time: (1) bare lands; (2) water bodies; and (3) snow. The values in Table 1 were
232 established after multiple tests before obtaining sufficient precision to distinguish **deposit zones** from other land
233 covers. On each mosaic (composite of the available images during the period of interest), a cloud mask is applied
234 using Landsat QA bands in the script to remove clouds from the scene.

235

$$\frac{\text{Band 4}-\text{Band 6}}{\text{Band 4}+\text{Band 6}}$$

Equation 1

236

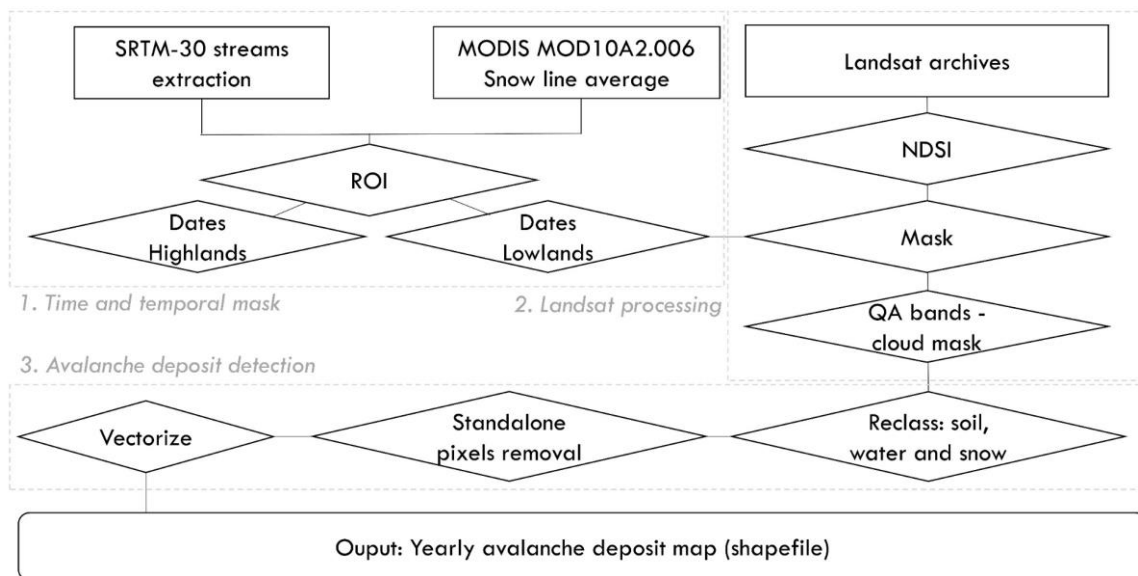
237 **Table 1. NDSI discrete values for avalanche **depositional zone** detection**

Coverage	NDSI values
Bare soil	-1 to -0.05
Water bodies	-0.051 to 0.30
Snow cover	0.31 to 1

238

239 *2.11 Depositional zone selection*

240 This further step reclassifies annual NDSI layers using ranges of values in Table 1. Only ‘snow cover’ that
 241 designates snow avalanche **deposit zones** is selected in the script. From the selected reclassification, the script
 242 removes the standalone pixels because their classification might not be precise or representative of actual cover.
 243 Next, the selected ‘avalanche pixels’ are verified into the script avoiding manual vectorization after the
 244 downloading process. The vectorization procedure of **depositional zones of avalanches** is justified by the analysis
 245 steps and post-processing after downloading data. **Depositional zones of avalanche** statistics, elevations, and
 246 **surface areas** are extracted from vector files. Finally, annual **avalanche deposit zone** shapefiles are exported into
 247 the Google Drive user’s account.



248
 249 **Figure 3. Flow chart for Snow Avalanche Frequency Estimation (SAFE) using Landsat archives in Google**
 250 **Engine.**

251
 252 *2.12 Depositional zones of avalanche surface area classification*

253 Once the data are downloaded and imported into the GIS environment, statistical analysis commences. Every year,
 254 the number and areas of **deposit zones** are calculated to quantify their evolution. Moreover, the **surface areas** of
 255 the **depositional zones** are classified. Although a generic **surface area** classification exists (Greene et al., 2016),
 256 we decided to classify avalanches by **surface areas** based on local conditions. We segregated four discrete
 257 categories of **deposit zones**: small (< 1000 m²); medium (1000-5000 m²), large (5000-15,000 m²), and very large
 258 (15,000-100,000 m²). Such a classification enabled us to assess the intensity and potential impact of those hazards

259 in specific locations. SAFE is not able to detect the avalanches at their time occurrence, and since these hazards
260 are detected weeks after initiation, their **surface area** is underestimated by SAFE due to melting. However, the
261 estimated **surface areas** in SAFE are still useful for classifying **depositional zones of avalanches** by **surface area**
262 since large snow deposits melt slower than small snow deposits. The small avalanches that occurred in winter will
263 appear as small deposit at the time of extraction in SAFE and the large events as large hazards since visible snow
264 deposits can be seen in late spring.

265

266 **3. Results**

267 *3.1 Validation*

268 The performance of SAFE in correctly detecting snow avalanche depositional zones required careful assessment.
269 To achieve this, we collected datasets that show actual locations (Global Positioning System) of avalanches that
270 occurred in the Amu Panj basin during the last 32 years. A total of 158 snow avalanche depositional zones were
271 easily identified in the riparian buffer zones on Google Earth images in 2001, 2003, 2015, 2017, and 2019. **No**
272 **other Google Earth images were available during the last 32 years in Afghanistan, therefore the comparison**
273 **between SAFE and the true events was conducted with those available 158 deposit zones. These 158 deposits were**
274 **extracted from Google Earth and stacked with SAFE outputs. Deposits identified by SAFE were considered valid**
275 **when the two datasets overlapped at the same location and when more than half of the polygon surfaces extracted**
276 **from SAFE overlapped the actual deposits visible on Google Earth images.** Here we used statistical measures to
277 assess the performance of SAFE through the Probability of Detection (POD; Equation 2, based on (Hafner et al.,
278 2021)):

279

$$280 \quad POD = \text{true positive deposit zones} / (\text{true positive deposit zones} + \text{false negative deposit zones})$$

281

Equation 2

282

283 where *true positive deposit zones* are the avalanches detected by SAFE that were actually visible on Google Earth
284 images (in valleys where GE images were available) and *false negative deposit zones* are the locations where SAFE
285 did not detect **deposit zones** that had actually happened. Moreover, Positive Predictive Value (PPV; Equation 3)
286 was calculated to assess the number of times SAFE found an actual **avalanche deposit zone** on the ground as
287 follows:

288

$$289 \quad PPV = \text{true positive deposit zones} / (\text{true positive deposit zones} + \text{false positive deposit zones})$$

290

Equation 3

291

292 where *false positive deposit zones* are avalanche **deposits predicted** by SAFE that had never occurred.

293
294 The results suggest a good reliability of SAFE (Table 2). The overall POD is 0.77 which means that SAFE
295 identified a significant number of the **depositional zones of avalanches** that impacted valley bottoms. Moreover, it
296 seems that SAFE performs better in detecting true positive **deposit zones** (that occurred on the ground), as shown
297 by the high PPV scores (average: 0.96). SAFE almost never detected **depositional zones of** avalanches that did not
298 exist. However, SAFE might miss some **deposit zones** due to cloud cover on the Landsat images, especially in
299 2001 (Table 2; POD = 0.42 in 2001).

300

301 **Table 2. Probability of detection and Positive Predictive Values of SAFE**

Statistics	2001	2003	2015	2017	2019	Average
True positive	10	35	12	19	48	
False negative	14	6	1	4	9	
False positive	1	0	0	1	3	
POD	0.42	0.85	0.92	0.83	0.84	0.77
PPV	0.91	1.00	1.00	0.95	0.94	0.96

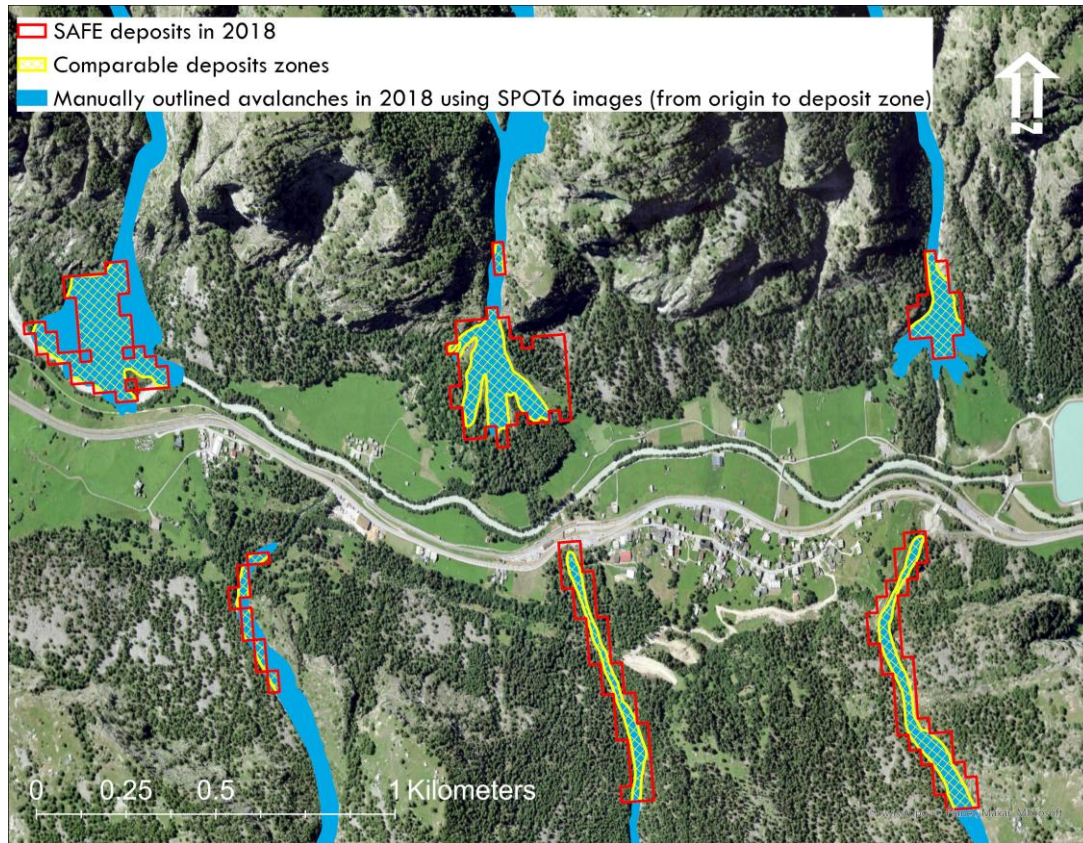
302

303 Another source of error arises when SAFE cannot detect **depositional zones** due to a dark color on the snow surface
304 associated with surface debris or a debris flow on top of the **deposit zones**. NDSI may have identified those debris
305 layers as bare soil in the classification. **Moreover, it should be understood by the users that another limitation is**
306 **that SAFE does not detect early winter avalanche deposits due to melting and snow coverage on and around the**
307 **snow deposit, which might affect the deposits frequency estimations. However,** based on our findings, SAFE can
308 be considered as a conservative, yet robust and efficient tool to automatically identify snow avalanche depositional
309 zones in very remote areas and can be applied in any mountainous region.

310

311 *3.2 SAFE outputs compared with outlined avalanches using SPOT-6 images*

312 **As a potential method of strengthening our testing of SAFE, outputs of our model were compared with a method**
313 **that applied a more precise and expensive remote sensing product in Switzerland in 2018 (Bühler et al., 2019b;**
314 **Hafner and Bühler, 2018). The Swiss area encompassed 12,500 km² where more than 18,000 snow avalanches**
315 **were manually digitized using very high-resolution SPOT-6 images (in January 2018). While our dataset is quite**
316 **different from the Swiss data, the objective of this comparison was to assess how many snow avalanche deposits**
317 **SAFE could detect compared to the approach using SPOT-6 (Table 3). Figure 4 shows an illustration of this**
318 **comparison. It appears that the deposit zones detected by SAFE are in line with SPOT6 outlined avalanches. The**
319 **later however covers the entire avalanches while SAFE only detects, automatically, the deposit zones.**



320
321 **Figure 4. An illustration of the comparison between automatic detection of deposit zones using Landsat**
322 **archives in SAFE and manually outlined snow avalanches (from origin to deposit zones) using SPOT6**
323 **images in Switzerland.**

324
325 **Table 3. Comparison of snow avalanches deposits zones between SAFE outputs (April to June 2018) and**
326 **manual digitization using high-resolution SPOT-6 images in Switzerland in January 2018***

Method	Number of snow polygons	Area of snow polygons (m²)
SPOT digitization	7574	362,187,741
SAFE detection	9948	494,454,599
Overlapping SPOT-SAFE	2194	223,907,868

327 *SPOT data based on (Bühler et al., 2019b; Hafner and Bühler, 2018)

328
329 **Importantly, not all avalanches manually digitized on SPOT-6 images were comparable to SAFE results. To make**
330 **this comparison more consistent, we clipped the outlined avalanches with the valley bottom mask used in SAFE.**
331 **Following this modification, the SPOT-6 digitization process identified 7574 avalanches deposits in valley bottoms**

332 compared with 9948 by SAFE. Overlapping these two datasets, we found that both approaches detected 2194
333 deposit zones in common. Much of this discrepancy is due to the timing of SAFE images, which examine deposits
334 that remain in late spring and early summer, whereas SPOT digitization covered only January. The larger number
335 of snow deposits detected by SAFE occur during late season snow avalanches that impact valleys. This suggests
336 that SAFE could not detect all January snow deposits because many of those already melted by the time of SAFE
337 detection (early April to late June in the Swiss case). In addition, optical image quality strongly depends on cloud
338 cover that may cause avalanches to be obstructed. For instance, we could not compare the 2019 SPOT-6 derived
339 dataset in eastern Switzerland (Hafner et al., 2021) due to cloudy images at the end of winter and early spring
340 because these snow avalanches had already melted, implying that SAFE is more suitable for high mountain areas
341 (>4000 m) where snow deposits remain longer in valleys, thus inflicting greater damages and obstructions. Using
342 LANDSAT images, SAFE somewhat circumvents this problem of cloud cover by assessing many years of data
343 (in our case 32 years). However, SAFE does not distinguish individual events and considers overlapping snow
344 deposits as one, in contrast to SPOT-6 which distinguishes these as discrete events. This, in addition to the different
345 methods and spatial resolution difference between SAFE and SPOT, explains the somewhat low number of
346 overlapping snow deposits between SAFE and SPOT. Moreover, the SPOT digitization procedure found a total
347 avalanche area of 362,187,741 m² in January, while SAFE detected 494,454,599 m² of deposits at the end of the
348 avalanche season, including 223,907,868 m² in common. The area detected by SAFE is naturally larger than SPOT-
349 6 since SAFE maps all detectable deposits at the end of the winter. Moreover, SAFE did not detect the small
350 avalanches of January that rapidly melted after they occurred. The polygons extracted by SAFE using Landsat
351 images are obviously coarser than those outlined with SPOT-6 images, which partly explains the low number of
352 overlapping snow deposit zones, but a much more comparable detected area (62%) between the two methods.
353 Much of the discrepancy is related to SAFE's inability to detect individual events and missing deposits that rapidly
354 melt (mostly from the early winter snow avalanches), as well as the very different resolution of these products.

355

356 3.3 Snow avalanche *depositional zone* frequency from 1990 to 2021

357 By compiling 32 years of satellite images (see Methodology), the frequency of avalanche *deposits* at a 900 m²
358 pixel scale was determined (Figure 5 and 6a). SAFE inventories snow avalanche *deposits* that occurred within a
359 year and therefore identifies the most vulnerable areas, but it does not aim to forecast the timing of future
360 avalanches. During this period, some 810,000 *depositional zones* impacted valleys within the Amu Panj basin
361 (28,500 km²), i.e., approximately 28 *depositional zones* km⁻². Each year these avalanche deposits cover an average
362 of 1.23% of the basin area but *surface area* varies from year to year. Avalanche *depositional zone surface area*
363 ranged from 900 to 100,000 m² and is categorized into four classes: small (< 1000 m²); medium (1000-5000 m²),
364 large (5000-15,000 m²), and very large (15,000-100,000 m²). The most frequent are medium-size *surface area*

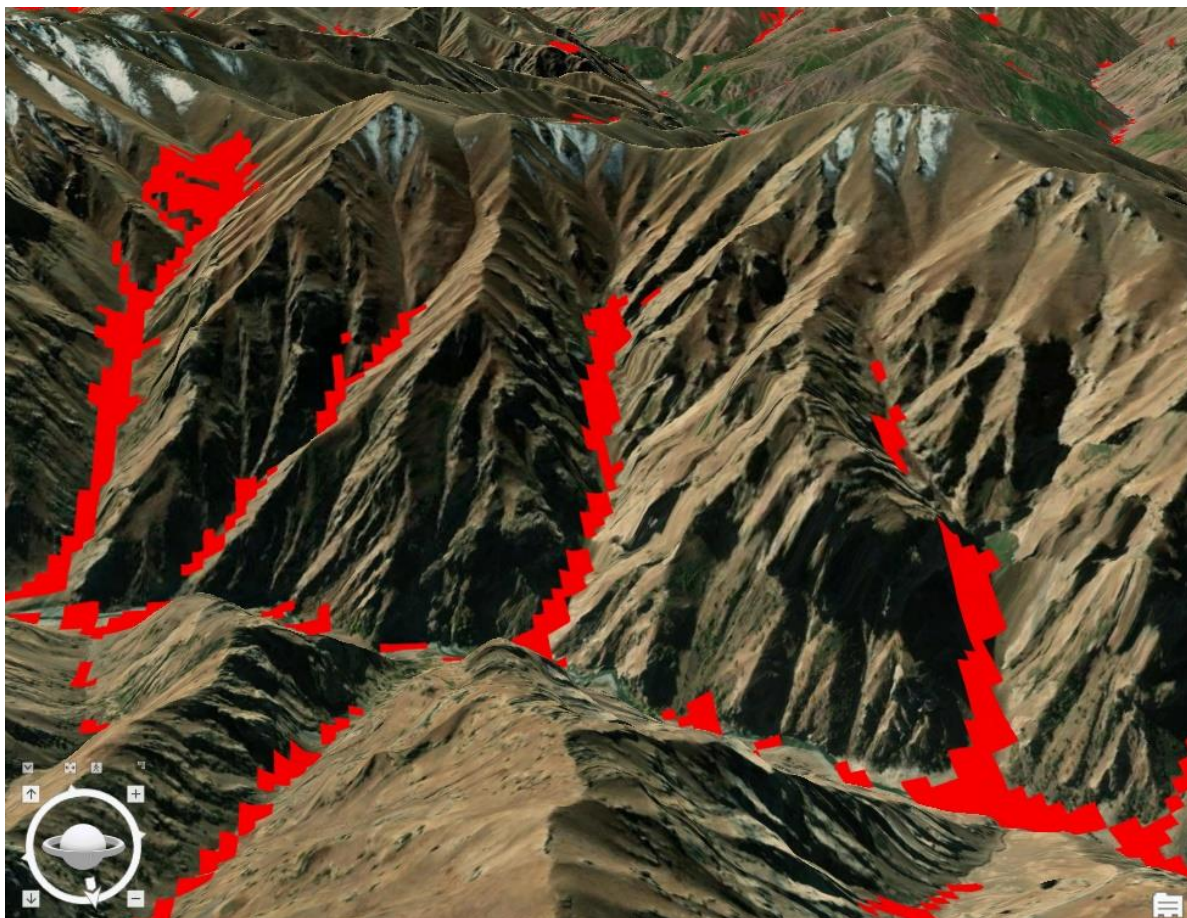
365 **deposit zones**; 342,000 events during the past 32 years. Our approach also identifies very large snow avalanche
366 **depositional zones** that pose the greatest danger to local populations and infrastructure. We found no correlation
367 between altitude of depositional zones and their **surface areas**. Avalanches deposits in this region have an average
368 altitude of 3820 m and the lowest **depositional zone** occurred at 1755 m.

369

370 These spatial and temporal statistics allow for a geographic assessment of the avalanche **deposits**. In total, ten sub-
371 catchments (ranging from 18 to 240 km²) were impacted by more than one avalanche **depositional zone** km⁻²y⁻¹,
372 with an average frequency of 0.26 **deposit zones** km⁻²y⁻¹ throughout the Panj Amu basin (Figure 7). More
373 importantly, these maps prioritize villages prone to avalanches **deposits** and inform relevant stakeholders which
374 villages and infrastructure are most at risk. Of the 4154 villages in the region, 50 are impacted by at least one
375 avalanche within a 1 km radius each year (Figure 8). These susceptible villages are in Upper Badakhshan in the
376 north of our study area and in the Wakhan Corridor in the east where the highest mountains and most remote
377 villages are located. During the 32-y period, 92 villages were affected by very large avalanches **depositional zones**
378 in Badakhshan and Wakhan. Since 2019, Aga Khan Agency for Habitat (AKAH) is monitoring villages of
379 Afghanistan that have been impacted by snow avalanches. In total, 217 villages have been impacted by avalanche
380 **deposit zones** and those are located in the same vulnerable valleys detected by SAFE, namely High Badakhashan
381 and the Wakhan corridor.

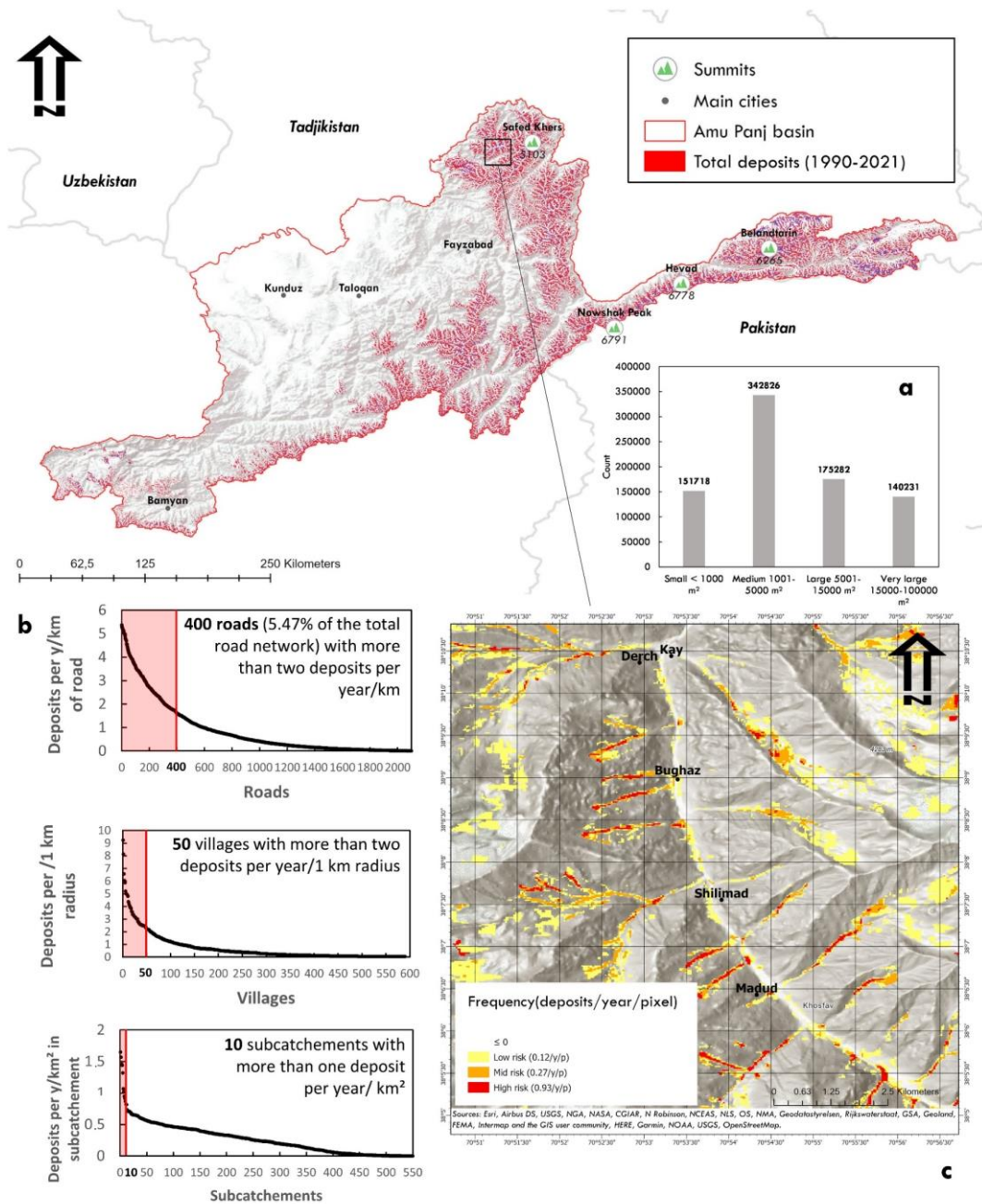
382

383 Our remote sensing approach facilitates innovation in snow avalanche **depositional zone** monitoring: i.e., detecting
384 avalanches **deposits** outside of populated areas, especially along roads that are frequently blocked by avalanches
385 (Figure 9). More than 2000 roads in the basin (5.47% of the road network) were affected by avalanche **deposits**
386 every year. Additionally, more than 400 roads in Upper Badakhshan and Wakhan regions experienced more than
387 2 avalanche **deposits** y⁻¹ km⁻¹ of road (within a 1 km buffer). The average frequency along roads is 0.86 avalanche
388 **deposits** km⁻¹y⁻¹ during the past 32 years, most of these in the medium-size **surface area** category.



389
390
391
392

Figure 5. 3-Dimensional view of the 32 years avalanche **depositional zones** in Khinj village, Afghanistan
(ArcGisPro)



393

394

395

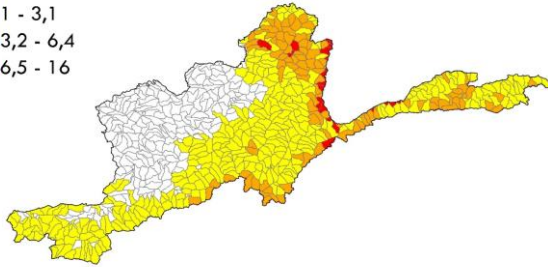
396

397

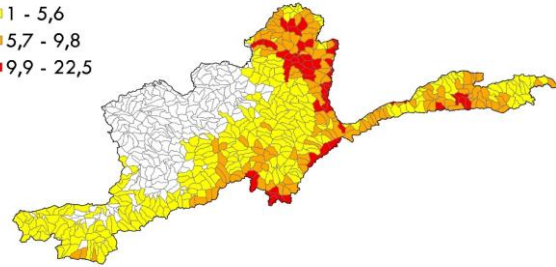
Figure 6. Yearly inventory map of snow avalanche depositional zones in the Amu Panj basin: 1990-2021: a, Surface area classification of avalanche depositional zone frequency; b, Avalanche depositional zone frequency per number of roads, villages, and subcatchments in the basin; c, An example map of avalanche depositional zone frequency during the 32-y period at a village scale.

Total snow avalanches deposits per km² in subcatchments (category 1) Total snow avalanches deposits per km² in subcatchments (category 2)

□ 0
■ 1 - 3,1
■ 3,2 - 6,4
■ 6,5 - 16



□ 0
■ 1 - 5,6
■ 5,7 - 9,8
■ 9,9 - 22,5



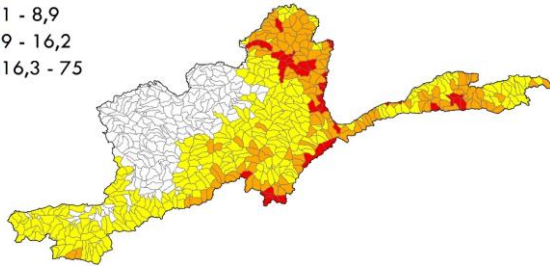
90 45 0 90 180 270 360
Kilometers



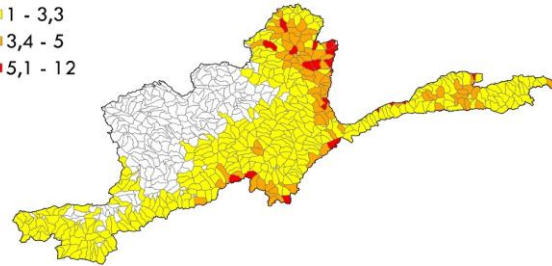
398

Total snow avalanches deposits per km² in subcatchments (category 3) Total snow avalanches deposits per km² in subcatchments (category 4)

□ 0
■ 1 - 8,9
■ 9 - 16,2
■ 16,3 - 75



□ 0
■ 1 - 3,3
■ 3,4 - 5
■ 5,1 - 12



399

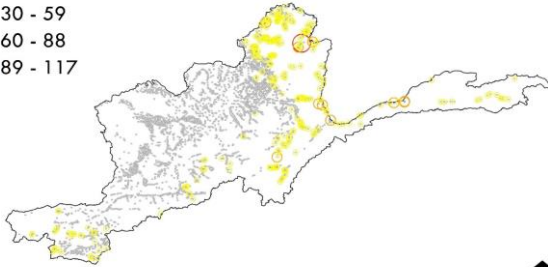
400

401

Figure 7. Total avalanche **depositional zones per category and per square kilometer in subcatchments during the past 32 years.**

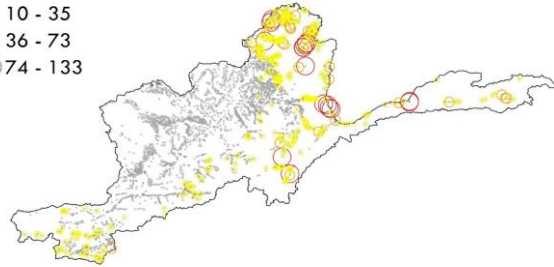
Total snow avalanches deposits per village (category 1)

- 0
- 30 - 59
- 60 - 88
- 89 - 117



Total snow avalanches deposits per village (category 2)

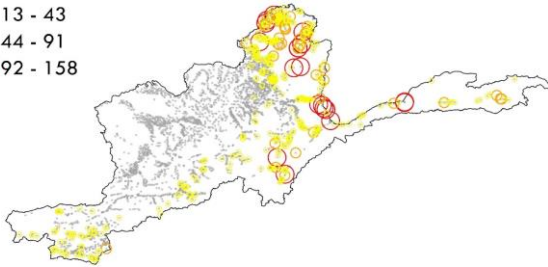
- 0
- 10 - 35
- 36 - 73
- 74 - 133



402

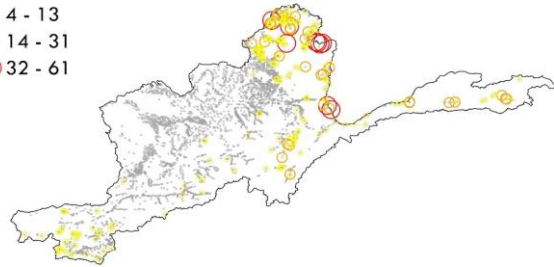
Total snow avalanches deposits per village (category 3)

- 0
- 13 - 43
- 44 - 91
- 92 - 158



Total snow avalanches deposits per village (category 4)

- 0
- 4 - 13
- 14 - 31
- 32 - 61



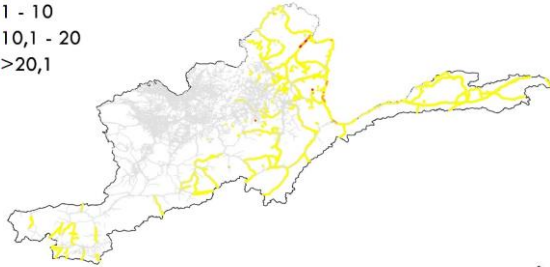
403

404

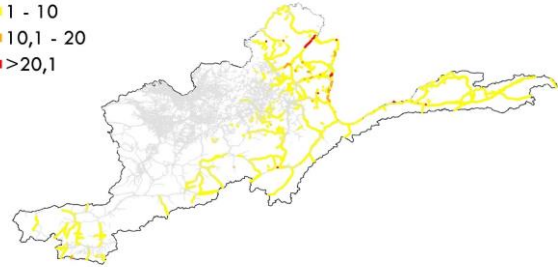
Figure 8. Total avalanche **depositional zones** per category and per village during the past 32 years.

Total number of avalanches deposits per kilometer of road (category 1) Total number of avalanches deposits per kilometer of road (category 2)

0
1 - 10
10,1 - 20
>20,1



0
1 - 10
10,1 - 20
>20,1



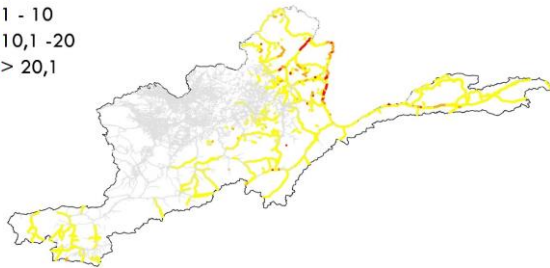
90 45 0 90 180 270 360
Kilometers



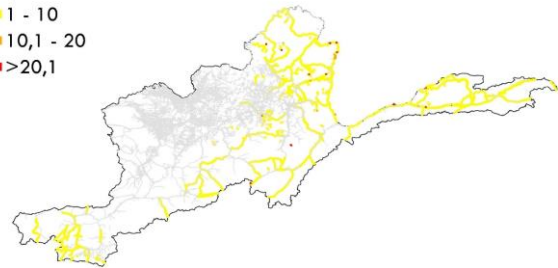
405

Total number of avalanches deposits per kilometer of road (category 3) Total number of avalanches deposits per kilometer of road (category 4)

0
1 - 10
10,1 - 20
> 20,1



0
1 - 10
10,1 - 20
>20,1



406

407 **Figure 9. Total avalanche **depositional zones** per category and per kilometer of roads during the past 32**
408 **years**

409

410

411

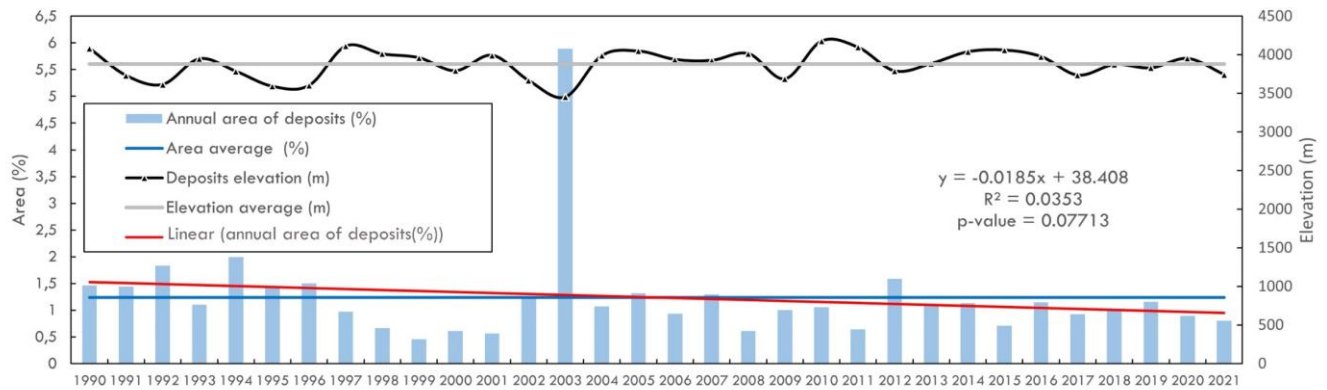
412

3.4 Stream blocking and resultant flooding

415 Damages to infrastructure and blocking of roads by avalanche deposits are not the only consequences of these mountain hazards. Because depositional zones typically reach rivers in this steep, incised terrain, the sudden and rapid arrival of several tons of snow can temporarily block rivers inducing short-term localized flooding. By cross-checking the map of the rivers in the Amu Panj basin with SAFE outputs, it appears that 26.2% of the river network is impacted by avalanche deposits, mainly in the high mountains. During the past 32 years, 12% of the streams have been blocked by at least 10 avalanche deposits km¹ representing a significant risk for villages and farms in floodplains. The accumulated snow mass impounds river water until it can break through releasing a large discharge surge. Thus, depending on the surface area of the avalanche deposit with respect to the channel dimensions, damages to villages and farmlands may occur both upstream due to impounded water (hours to weeks) and to downstream following the sudden release of water.

425 3.5 Snow avalanche depositional zone trends during the past 32 years

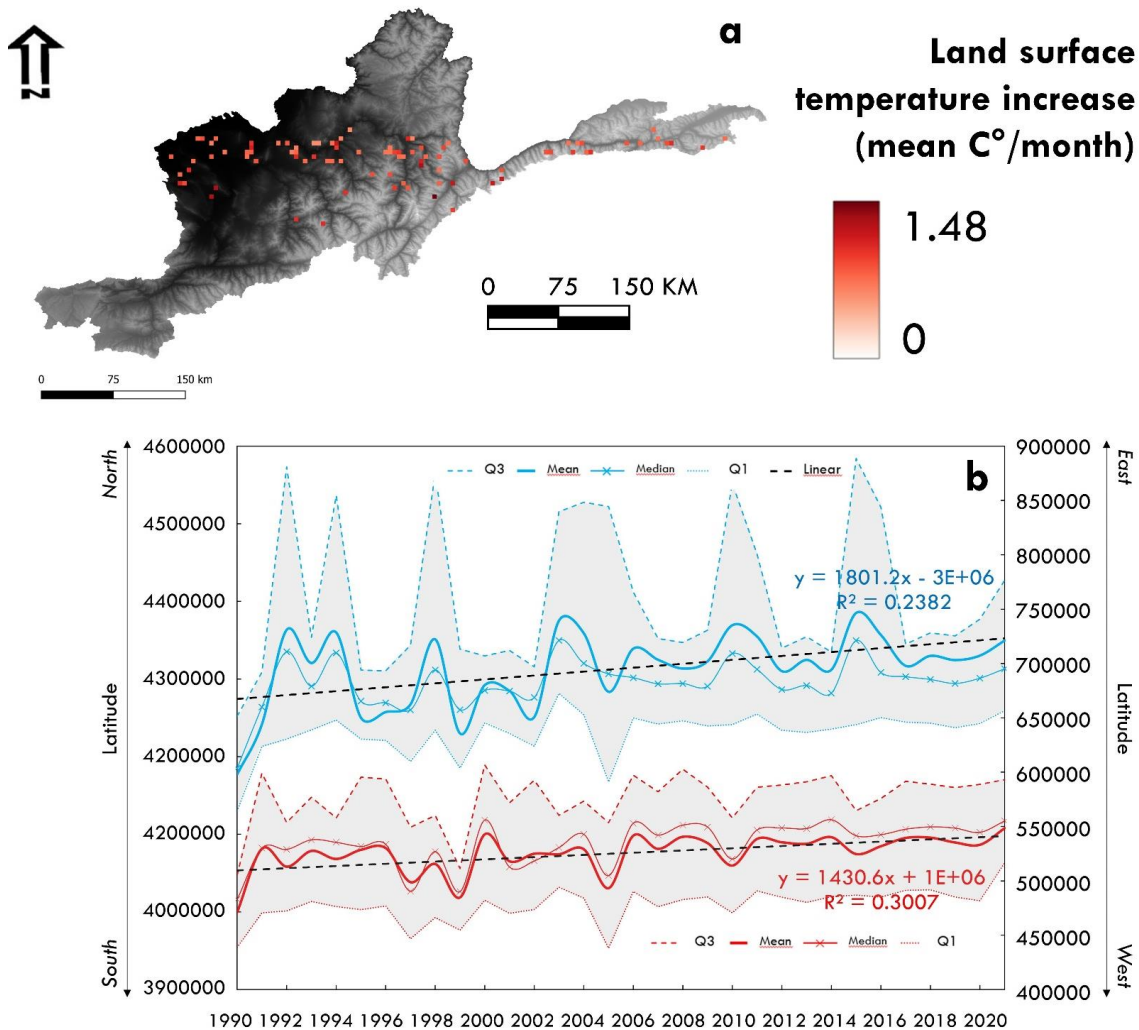
This long-term monitoring of snow avalanche deposits facilitates the assessment of the evolution of these rapid mass movements. During the 32 years of avalanche depositional zone assessment, no significant temporal trends in impacted areas were detected (Figure 10). In addition, there was no significant trend of the surface area of snow deposits (p-value > 0.05). Nevertheless, some years posed much greater risk than others. In the last 32 years, ten years have been more at risk with above-average avalanche deposit coverage: 1990, 1991, 1992, 1993, 1994, 1995, 1996, 2003, 2005, 2007 and 2012. In particular, 430 2003 had many avalanche depositional zones that occupied almost 6% of the surface area of the entire basin. That year was locally noted as having heavy snowfall and farmers benefited from more snowmelt in the spring, leading to higher than average crop yields in 2003 (FAO, 2003; Guimbert, 2004). Notably, the higher risk years were also characterised by lower altitudes for avalanche deposits. There is a slight negative correlation (-0.55, Pearson test) between altitude and total annual avalanche area. 435 With larger avalanche areas, deposits reach closer to villages. For example, in 2003, the lowest avalanche depositional zone occurred at an altitude of only 1871 m, very close to housing clusters and roads. It is therefore possible that communities below 2000 m are also impacted by snow avalanche deposits and in many mountain regions of the world this represents a significant proportion of the communities living proximate to these altitudes.



440 **Figure 10. Snow avalanche *depositional zone* area and elevation trends since 1990 in the Amu Panj basin. Elevation**
was calculated within each polygon of avalanche *deposits* using SRTM-30 Digital Elevation Model. Mann-Kendall p-
value 0.05 test was conducted to assess the significance of the trend.

3.6 Temporal geographic shifts of snow avalanche *deposit zones*

445 Long-term monitoring also shows the evolution of the spatial distribution of snow avalanche *depositional zones*. The pattern
of snow avalanche *deposits* has changed with time and slightly shifted to the northeast portion of the basin; thus, more
avalanches are now occurring in the northeast than in the southwest (Figure 11 a and b). Nevertheless, snow coverage did not
shift simultaneously according to our remote sensing analysis nor did the snowline evolve, but rather remained variable over
the last 32 years. The geographic shift of avalanche *depositional zones* is therefore likely due snow depth evolution. Deeper
450 snowpacks trigger snow avalanches. There are no available data on snow depth at such a scale. *However, the slope of the*
temperature was calculated and a Mann-Kendal test was applied for each pixel of the land surface temperature images
(MOD11C3). Remotely sensed land surface temperature changed during the last 20 years (Figure 11 a), with a warmer band
occurring through the central portion of the basin in December (p-value 0.03 with an increase of 0.88 C°y⁻¹). This central
portion is mainly mountainous, and this temperature pattern may have shifted the avalanches to the northern mountains of the
455 area, while the south is characterized by lower mountains. Overall, avalanche *depositional zone* locations tend to follow the
spatial distribution of snow depth (Bühler et al., 2016). This means that despite the high variability of the snow line and snow
coverage, the distribution of snow avalanche *deposits* can significantly change over time in response to temperature changes
and local communities must be prepared for shifting hazards.



460 **Figure 11. a, Map of areas with significant increases in monthly land surface temperatures in the Amu Panj Basin based on MOD11C3 products from 2000 to 2021; b, Geographical shift of avalanche deposits: mean longitude and latitude of avalanche deposits each year since 1990 show evidence of a movement to the northeast due to increasing winter temperature in mountainous areas.**

465 **4. Uncertainties and implications**

4.1 Sensitivity analysis of SAFE

To better understand how SAFE works and assess its performance, a sensitivity analysis was conducted between the model parameters. The number and surface areas of avalanche depositional zones vary according to the buffer used, the dates of Landsat images, and finally the NDSI range during the snow classification. The sensitivity analysis was conducted for the year 470 2019 when SAFE was most robust in valleys where actual avalanche deposits were quite visible on Google Earth images

(POD: 0.84 and PPV: 0.94). First, we run SAFE with different buffer widths (25 m of difference between each buffer). There is a strong positive correlation (0.98) between the number of avalanche **deposits** detected by SAFE and the buffer width (Figure 12a). The wider the buffer around the rivers, the more avalanche **deposits** SAFE will detect. On the other hand, for narrower buffers, the average surface area of avalanche **depositional zones** is smaller (positive correlation of 0.71). This is because a large buffer extends upslope where small snow patches reside, which are not avalanche **deposits** since they are located at the top of hillslopes. This means that the user should not select a buffer that is too wide, rather the area should only include the riparian zone of rivers and streams where the snow avalanche deposits are located. As such, we used a value of 200 m for the entire region studied.

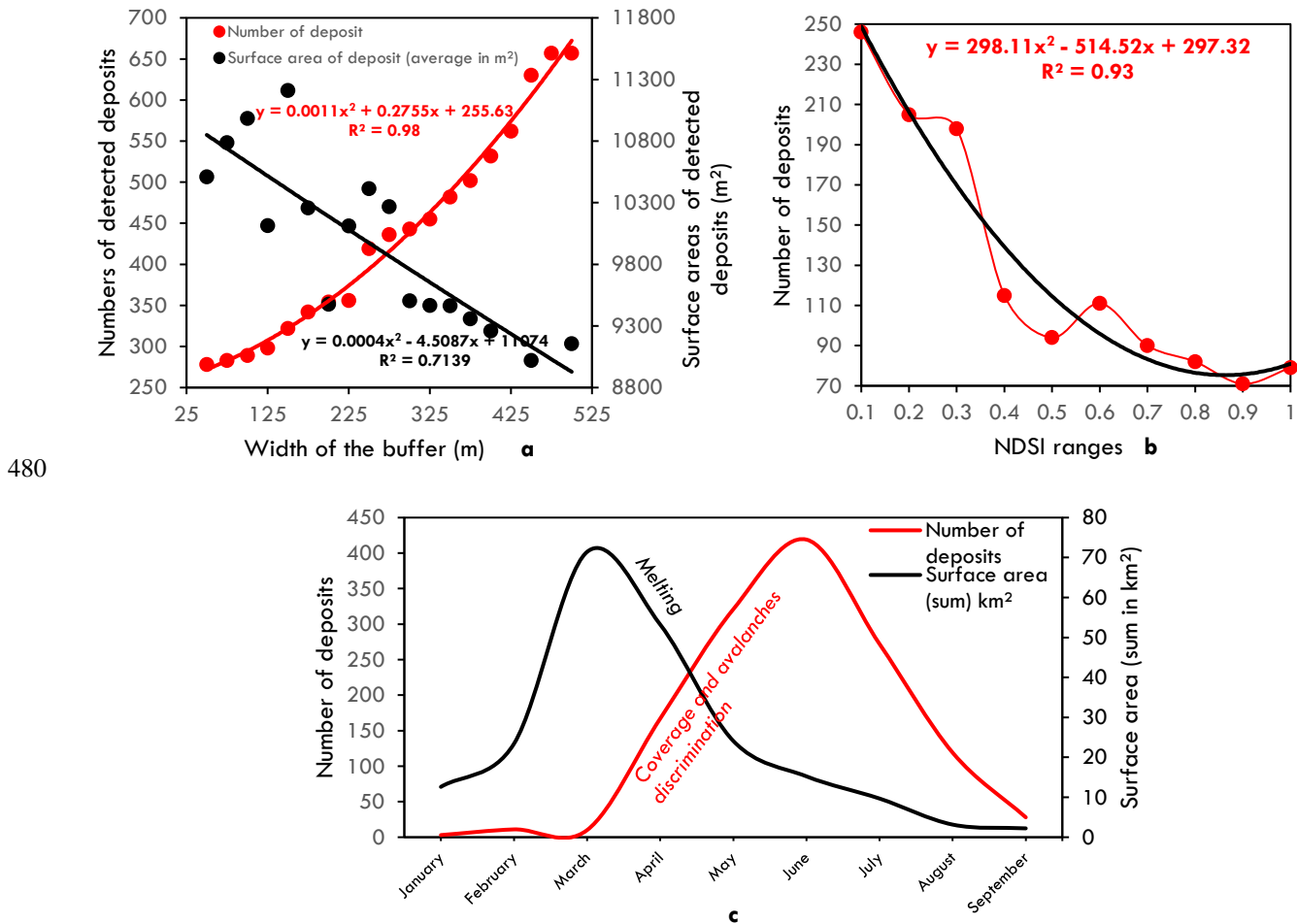


Figure 12. Sensitivity tests of SAFE for number and surface areas of detected avalanche depositional zones: a, width of buffer; b, NDSI ranges; and c, dates of interest

485 The number and **surface areas** of avalanche **depositional zones** detected by SAFE depends on the NDSI range when classifying
snow. NDSI is used to differentiate between water bodies, bare lands, and snow. By varying the NDSI ranges of snow in the
script, we notice a strong positive correlation with the number of avalanche **deposits** detected by SAFE. The closer the index
is to 0, the more hazards SAFE finds. However, this correlation shows that the choice of NDSI range is important because we
notice a threshold at 0.31 (Figure 12b). Avalanche **depositional zones** seem to be more numerous with an NDSI lower than
490 0.31 because the snow pixels are confused with water bodies. It is therefore essential for the user to select an NDSI higher than
0.31 to distinguish water bodies (rivers, flood areas or lakes) and snow. However, there is no correlation between the NDSI
ranges and the average surface areas of avalanche **deposits** because NDSI cannot interpret pixels other than 'snow' above the
0.31 threshold. Finally, the date of interest is a key parameter in SAFE. The number of avalanche **depositional zones** detected
by SAFE is highest at the end of winter due to the almost constant cloud cover since January, but also due to the inability to
495 distinguish avalanche **deposits** from snow cover in winter (with Landsat images) (Figure 12c). May is a key month for SAFE
applications in high mountains: the snow coverage, which is thinner than the avalanche **depositional zones**, begins to melt and
the number of avalanche **deposits** detected can then be assessed. It is therefore essential to select post-May images to detect
avalanche **deposits** while taking care not to select post-July images as avalanches **deposits** melt in summer precluding detection.

500 Some avalanche deposits are also visible on successive images after the snow cover melts. SAFE was specifically designed to
detect avalanche **depositional zones** at their earliest stage after snow melts. Indeed, starting from May (when the avalanche
deposits are not confused with snow coverage), snow avalanche deposits start to melt and the **surface area will begin to** be
underestimated. For that reason, it is important to select late spring images for lowland avalanche **depositional zones** and early
summer for highland **deposits**, not later. Cloud cover is another issue in avalanche **deposit** locations and **surface area** detection
505 since cloud cover may partly or fully obstruct the avalanche **deposits** at the time of the image. This is another reason to select
images starting from late spring when regional cloud cover is lowest and even absent in early summer. If cloud cover is high
even late spring, the users can still select later images, but there will be a risk that detected avalanche deposits will have started
to melt. To summarize, we recommend the following three parameters in the SAFE script: buffer of 200 m to include only
snow avalanche deposits; NDSI > 0.31 to distinguish water bodies from snow, and images from May to July to distinguish
510 avalanche **depositional zones** from snow cover.

4.2 Excluding snow coverage

Interpreting the remaining snow packages as avalanche deposits can lead to some errors. Indeed, despite a precise masking
operation (excluding summits and very high plateaus where snow persists), in some cases the use of NDSI might not properly
515 segregate avalanche **depositional zones** from large areas of remaining snow. After assessing the **surface area** of true avalanche
deposits (the ones that SAFE correctly detected based on Google Earth images), it appeared that snow cover areas > 100,000
m² were not avalanche **depositional zones** but rather only snow cover; thus, these were removed. However, in highlands, even
along riverbanks, some snow packages interpreted as avalanche **depositional zones** may be remaining snow cover. As such,

the date range for highlands was selected as late as possible in the year. Thus, it is advised to keep the mask at the very bottom
520 of valleys (maximum 200 m buffer along the river) to exclude high plateaus and potential snow-covered areas.

4.3 Water bodies in SAFE

A final limitation of using this remote sensing and NDSI approach for avalanche **deposit** detection is the possible confusion
525 between some small water bodies and avalanche **depositional zones**. Indeed, in some cases certain river reaches (stream order
> 4 in our study area) could be interpreted as snow because they were frozen and appeared as white pixels on Landsat archives.
The same issue can occur with ponds and lakes. This limitation was foreseen before processing the images in our study and
we excluded these large water bodies from the region of interest (in the mask) by using available shapefiles. For example,
Shiva Lake, one of the largest water bodies in Amu Panj basin (15 km²), was removed from the analysis. Another way to avoid
the water pixel selection is to adapt the NDSI reclassification itself, depending on the study area. This is possible in the script
530 lines 51-53 for low elevations and lines 139-141 for high elevations in the script.

4.4 SAFE outcomes compared to other snow avalanches detection studies

SAFE contributes to the literature on snow avalanche detection, but in a unique way using remote sensing. As noted, many
studies and models exist using various products: radar, optical, and topographic. The strength of remote sensing is the automatic
535 processing across wide scales and over long timeframes. SAFE uses the capabilities of remote sensing by processing more
than one image per year at the catchment scale. Moreover, the use of Landsat archives allows assessment over the last 32 years,
which is not yet possible with recent radar data such as Sentinel-1. Most of the current avalanche detection models use freely
available products, with acceptable if not good accuracy (Table 4). The accuracy of these studies using radar images ranges
from 53 to 81% making this a relatively robust tool. One of the reasons why SAFE does not use radar images is the weight of
540 the images (data storage), especially Sentinel-1, which is mostly above 1 Gb/image. These heavy images are not suitable for a
model like SAFE, which was specifically designed for remote study areas where internet connections may be very limited.
Other models also exist with optical images with high accuracy ranging from 71 to 93% (Table 4). In the optical domain,
SAFE showed a POD of 77% over an area of 28,500 km². SAFE is therefore in the high range of models with optical, medium
resolution (Landsat) images.

545

550

Table 4. References on snow avalanche accuracy using remote sensing products (Radar, Optical and Terrain)

Reference	Accuracy (%)	Dataset
Malnes et al., 2015	53*	S1
Vickers et al., 2016	60	S1
Leinss et al., 2020	70	S1 and TerraSAR-X
Karas et al., 2021	70	S1
Hafner et al., 2021	74**	SPOT
Eckerstorfer et al., 2017	75	S1
Yang et al., 2020	75**	S1
Martinez-Vazquez	76	GB-SAR LISA
Tompkin and Leinss, 2021	81	S1
Yarivan et al., 2020	90	Google Earth imagery
Singh et al., 2019	93	L8
Bühler et al., 2018	95**	DTM

*55 avalanches were detected using S1 image out of 102 on the field.

555 **POD

5. Conclusion

SAFE can be considered as a universal approach to assess snow avalanche **depositional zones in spring and early summer** where ground data are very limited, such as in the Afghan mountains. Here we showed the capability of long-term remote sensing data to robustly detect snow avalanche **deposits** that impact valley locations. While we have successively applied SAFE to assess the frequency and impacts of avalanche **deposits** in valleys and lower hillslopes of Afghanistan, arguably one of the most data-limited regions worldwide, this model should perform even better in areas where snow data are available making it an important tool for avalanche vulnerability assessment worldwide. More than 30 years after the launch of Landsat-5, it is now possible to compile all data and assess the temporal as well as spatial evolution of such hazards. NDSI is a relevant index to detect avalanches when selecting the correct region and dates of interest - i.e., riverbanks during the late melt season. The thickness of the depositional zones facilitates the detection of these avalanche deposits after the snow cover has melted on hillslopes in spring or early summer. **Moreover, the application of SAFE in Afghanistan, compared to its application in Switzerland, showed that the script can be applied worldwide, especially in high mountains (above 4000 m) since deposit zones are still detectable in late spring at those elevations.**

570

The automation of snow avalanche detection using remote sensing technologies at regional scales is still new and SAFE was designed to guide decision-makers, planners, and disaster risk practitioners. Indeed, such people can now know where the most at-risk areas are located based on these frequency maps. Such information informs the relative risk of building sites and land use decisions in such mountainous terrain with greater precision. The level of exposure of roads to avalanche **depositional**

575 **zones** can also be estimated using these frequency maps and can inform road planners and managers regarding road location, maintenance practices, and mitigation structures. **Moreover, villages of high mountains such as in Afghanistan are highly dependent on road access and connections to provide necessary food, energy, medical supplies, and life-support, especially in winter. It is therefore critical for local decision makers to assess the frequency of road blockage by avalanche deposits. Thus, open-access and user-friendly tools such as SAFE are highly applicable to interests of local stakeholders even with medium to**

580 **low power computers since SAFE uses Google servers.** The tourism sector can also benefit from this snow avalanche **deposit** inventory, especially the winter sports industry. Furthermore, this method can also be used to prioritize areas for more sophisticated and data-intensive avalanche risk analysis (Keylock et al., 1999). SAFE can be applied by any user throughout mountainous regions of the world as it is designed to be user-friendly, and frequent users can contribute to the robustness of the snow avalanche **deposit** archive, thus improving recommendations for policy makers.

585

Author contributions

A.C. designed the concept of SAFE method, wrote the Google Engine script and processed the analyses of snow avalanches. A.C. and R.C.S. participated the conception of SAFE and all authors helped interpret the results. D.R.G. contributed to the writing and provided the AKAH dataset of impacted villages by snow avalanches. A.C. and R.C.S. wrote the paper.

590

Competing interests

The authors declare that they have no conflict of interest.

Acknowledgements

595 The authors are very thankful to Nusrat Nahab, Head of Emergency Management Aga Khan Agency for the Aga Khan Agency for Habitat for her support in this study and for sharing information about snow avalanches in Afghanistan. This study was implemented under the ongoing project "Addressing Climate Change in Afghanistan (E3C)" funded by the European Union, in close collaboration with Aga Khan Foundation and Wildlife Conservation Society based in Afghanistan.

References

- 600 Abermann, J., Eckerstorfer, M., Malnes, E., Hansen, B.U., 2019. A large wet snow avalanche cycle in West Greenland quantified using remote sensing and in situ observations. *Nat Hazards* 97, 517–534. <https://doi.org/10.1007/s11069-019-03655-8>
- Asad Sarwar, Q., 2002. Water resources management in Afghanistan: the issues and options. International Water Management Institute, Pakistan.
- 605 Bair, E.H., Rittger, K., Ahmad, J.A., Chabot, D., 2020. Comparison of modeled snow properties in Afghanistan, Pakistan, and Tajikistan. *The Cryosphere* 14, 331–347. <https://doi.org/10.5194/tc-14-331-2020>
- Barbolini, M., Pagliardi, M., Ferro, F., Corradeghini, P., 2011. Avalanche hazard mapping over large undocumented areas. *Nat Hazards* 56, 451–464. <https://doi.org/10.1007/s11069-009-9434-8>

- 610 Bühler, Y., Adams, M.S., Bösch, R., Stoffel, A., 2016. Mapping snow depth in alpine terrain with unmanned aerial systems (UASs): potential and limitations. *The Cryosphere* 10, 1075–1088. <https://doi.org/10.5194/tc-10-1075-2016>
- Bühler, Y., Bebi, P., Christen, M., Margreth, S., Stoffel, L., Stoffel, A., Marty, C., Schmucki, G., Caviezel, A., Kühne, R., Wohlwend, S., Bartelt, P., 2022. Automated avalanche hazard indication mapping on a statewide scale. *Natural Hazards and Earth System Sciences* 22, 1825–1843. <https://doi.org/10.5194/nhess-22-1825-2022>
- 615 Bühler, Y., Hafner, E.D., Zweifel, B., Zesiger, M., Heisig, H., 2019a. Where are the avalanches? Rapid SPOT6 satellite data acquisition to map an extreme avalanche period over the Swiss Alps. *The Cryosphere* 13, 3225–3238. <https://doi.org/10.5194/tc-13-3225-2019>
- Bühler, Y., Hafner, E.D., Zweifel, B., Zesiger, M., Heisig, H., 2019b. Where are the avalanches? Rapid SPOT6 satellite data acquisition to map an extreme avalanche period over the Swiss Alps. *The Cryosphere* 13, 3225–3238. <https://doi.org/10.5194/tc-13-3225-2019>
- 620 Bühler, Y., von Rickenbach, D., Christen, M., Margreth, S., Stoffel, L., Stoffel, A., Kühne, R., 2018a. Linking modelled potential release areas with avalanche dynamic simulations: an automated approach for efficient avalanche hazard indication mapping. *International snow science workshop proceedings 2018* 810–814.
- Bühler, Y., von Rickenbach, D., Stoffel, A., Margreth, S., Stoffel, L., Christen, M., 2018b. Automated snow avalanche release area delineation – validation of existing algorithms and proposition of a new object-based approach for large-scale hazard indication mapping. *Natural Hazards and Earth System Sciences* 18, 3235–3251. <https://doi.org/10.5194/nhess-18-3235-2018>
- 625 Chabot, D., Kaba, A., 2016. Avalanche forecasting in the Central Asian countries of Afghanistan, Pakistan and Tajikistan. Presented at the International Snow Science Workshop, Breckenridge, Colorado.
- Colorado Avalanche Information Center, 2021. *Avalanche.org » Accidents* [WWW Document]. *Avalanche.org*. URL <https://avalanche.org/avalanche-accidents/> (accessed 6.30.21).
- 630 Deems, J.S., Painter, T.H., Finnegan, D.C., 2013. Lidar measurement of snow depth: a review. *Journal of Glaciology* 59, 467–479. <https://doi.org/10.3189/2013JoG12J154>
- Eckerstorfer, M., Bühler, Y., Frauenfelder, R., Malnes, E., 2016. Remote sensing of snow avalanches: Recent advances, potential, and limitations. *Cold Regions Science and Technology* 121, 126–140. <https://doi.org/10.1016/j.coldregions.2015.11.001>
- 635 Eckerstorfer, M., Malnes, E., Frauenfelder, R., Doomas, U., Brattli, K., 2014. Avalanche Debris Detection Using Satellite-Borne Radar and Optical Remote Sensing. *International Snow Science Workshop 2014 Proceedings, Banff, Canada* 131–138.
- Eckerstorfer, M., Malnes, E., Müller, K., 2017. A complete snow avalanche activity record from a Norwegian forecasting region using Sentinel-1 satellite-radar data. *Cold Regions Science and Technology, International Snow Science Workshop 2016 Breckenridge* 144, 39–51. <https://doi.org/10.1016/j.coldregions.2017.08.004>
- 640 European Avalanches Warning Services, 2021. *Fatalities* [WWW Document]. *EAWS*. URL <https://www.avalanches.org/fatalities/> (accessed 6.30.21).
- FAO, 2003. *FAO global information and early warning system on food and agriculture - world food programme* [WWW Document]. URL <https://www.fao.org/3/j0156e/j0156e00.htm> (accessed 10.17.21).
- 645 GFDRR, 2018. *Afghanistan Multi-Hazard Risk Assessment*. World Bank, Kabul, Afghanistan.
- Greene, E., Birkeland, K., Elder, K., McCammon, I., Staples, M., Sharaf, D., 2016. *Observation Guidelines for Avalanche Professionals in the U.S.* American Avalanche Association (No. ISBN-13: 978-0-9760118-1-1). Pagosa Springs, Victor, United States of America.
- 650 Gubler, H., 1987. Measurements and modelling of snow avalanche speeds, in: *Proceedings of the Davos Symposium*. Presented at the Avalanche Formation, Movement and Effects, Davos.
- Guimbert, S., 2004. *Structure and performance of the Afghan economy*. World, Washington D.C, United States.
- Hafner, E., Bühler, Y., 2018. *SPOT6 Avalanche outlines* 24 January 2018.
- Hafner, E., Lneiss, S., Techel, F., Bühler, Y., 2021. *Satellite avalanche mapping validation data* [WWW Document]. URL <https://www.envidat.ch/#/metadata/satellite-avalanche-mapping-validation> (accessed 3.23.22).
- 655 Hafner, E.D., Techel, F., Leinss, S., Bühler, Y., 2021. Mapping avalanches with satellites – evaluation of performance and completeness. *The Cryosphere* 15, 983–1004. <https://doi.org/10.5194/tc-15-983-2021>

- Hammond, J.C., Saavedra, F.A., Kampf, S.K., 2018. Global snow zone maps and trends in snow persistence 2001–2016. *International Journal of Climatology* 38, 4369–4383. <https://doi.org/10.1002/joc.5674>
- 660 Islamic Republic of Afghanistan Governmental Website, 2021. Badakhshan [WWW Document]. English. URL <https://president.gov.af/en/badakhshan/> (accessed 8.31.21).
- Keylock, C.J., McClung, D.M., Magnusson, M.M., 1999. Avalanche risk mapping by simulation. *Journal of Glaciology* 303–314.
- 665 Kravtsova, V.I., 1990. Snow Cover Mapping of Afghanistan’s Mountains with Space Imagery. *Mapping Sciences and Remote Sensing* 27, 295–302. <https://doi.org/10.1080/07493878.1990.10641815>
- Louge, M.Y., Turnbull, B., Carroll, C., 2012. Volume growth of a powder snow avalanche. *Annals of Glaciology* 53, 57–60. <https://doi.org/10.3189/2012AoG61A030>
- Maggioni, M., Gruber, U., 2009. The influence of topographic parameters on avalanche release dimension and frequency. *Cold Regions Science and Technology, ISSW 2002: International Snow Science Workshop* 37, 407–419. [https://doi.org/10.1016/S0165-232X\(03\)00080-6](https://doi.org/10.1016/S0165-232X(03)00080-6)
- 670 Malnes, E., Eckerstorfer, M., Vickers, H., 2015. First Sentinel-1 detections of avalanche debris. *The Cryosphere Discussions* 9, 1943–1963. <https://doi.org/10.5194/tcd-9-1943-2015>
- Martinez-Vazquez, A., Fortuny-Guasch, J., 2008. A GB-SAR Processor for Snow Avalanche Identification. *IEEE Transactions on Geoscience and Remote Sensing* 46, 3948–3956. <https://doi.org/10.1109/TGRS.2008.2001387>
- 675 Mohanty, A., Hussain, M., Mishra, M., Kattel, D.B., Pal, I., 2019. Exploring community resilience and early warning solution for flash floods, debris flow and landslides in conflict prone villages of Badakhshan, Afghanistan. *International Journal of Disaster Risk Reduction* 33, 5–15. <https://doi.org/10.1016/j.ijdr.2018.07.012>
- OCHA-United Nations, 2012. Districts Affected by Avalanches -Badakhshan Province 19Jan.2012.
- 680 Prokop, A., 2008. Assessing the applicability of terrestrial laser scanning for spatial snow depth measurements. *Cold Regions Science and Technology, Snow avalanche formation and dynamics* 54, 155–163. <https://doi.org/10.1016/j.coldregions.2008.07.002>
- Prokop, A., Schön, P., Singer, F., Pulfer, G., Naaim, M., Thibert, E., 2013. Determining Avalanche Modelling Input Parameters Using Terrestrial Laser Scanning Technology. *International Snow Science Workshop Grenoble – Chamonix Mont-Blanc - October 07-11, 2013* 770–774.
- 685 Schaffhauser, A., Adams, M., Fromm, R., Jörg, P., Luzi, G., Noferini, L., Sailer, R., 2008. Remote sensing based retrieval of snow cover properties. *Cold Regions Science and Technology, Snow avalanche formation and dynamics* 54, 164–175. <https://doi.org/10.1016/j.coldregions.2008.07.007>
- Singh, D.K., Mishra, V.D., Gusain, H.S., Gupta, N., Singh, A.K., 2019. Geo-spatial Modeling for Automated Demarcation of Snow Avalanche Hazard Areas Using Landsat-8 Satellite Images and In Situ Data. *J Indian Soc Remote Sens* 47, 513–526. <https://doi.org/10.1007/s12524-018-00936-w>
- 690 Singh, K.K., Singh, D.K., Thakur, N.K., Dewali, S.K., Negi, H.S., Snehmani, Mishra, V.D., 2020. Detection and mapping of snow avalanche debris from Western Himalaya, India using remote sensing satellite images. *Geocarto International* 0, 1–19. <https://doi.org/10.1080/10106049.2020.1762762>
- Smith, W.D., Dunning, S.A., Brough, S., Ross, N., Telling, J., 2020. GERALDINE (Google Earth Engine supRaglAciaL Debris INput dETector): a new tool for identifying and monitoring supraglacial landslide inputs. *Earth Surface Dynamics* 8, 1053–1065. <https://doi.org/10.5194/esurf-8-1053-2020>
- 695 Soteres, R.L., Pedraza, J., Carrasco, R.M., 2020. Snow avalanche susceptibility of the Circo de Gredos (Iberian Central System, Spain). *Journal of Maps* 16, 155–165. <https://doi.org/10.1080/17445647.2020.1717655>
- Tompkin, C., Leinss, S., 2021. Backscatter Characteristics of Snow Avalanches for Mapping With Local Resolution Weighting. *IEEE Journal of Selected Topics in Applied Earth Observations and Remote Sensing* 14, 4452–4464. <https://doi.org/10.1109/JSTARS.2021.3074418>
- 700 USAID, 2021. Afghanistan Avalanches [WWW Document]. URL <http://afghanistanavalanches.org/> (accessed 6.30.21).
- World Bank, 2017. Climate in Crisis: How Risk Information Can Build Resilience in Afghanistan [WWW Document]. URL <https://blogs.worldbank.org/endpovertyinsouthasia/climate-crisis-how-risk-information-can-build-resilience-afghanistan> (accessed 6.30.21).
- 705 Yang, J., Li, C., Li, L., Ding, J., Zhang, R., Han, T., Liu, Y., 2020. Automatic Detection of Regional Snow Avalanches with Scattering and Interference of C-band SAR Data. *Remote Sensing* 12, 2781. <https://doi.org/10.3390/rs12172781>

- Yariyan, P., Avand, M., Abbaspour, R.A., Karami, M., Tiefenbacher, J.P., 2020. GIS-based spatial modeling of snow avalanches using four novel ensemble models. *Science of The Total Environment* 745, 141008. <https://doi.org/10.1016/j.scitotenv.2020.141008>
- Zhang, J., Gurung, D.R., Liu, R., Murthy, M.S.R., Su, F., 2015. Abe Berek landslide and landslide susceptibility assessment in Badakhshan Province, Afghanistan. *Landslides* 12, 597–609. <https://doi.org/10.1007/s10346-015-0558-5>